JOURNAL OF AEROSPACE SOCIETY MALAYSIA

ARTICLE

GAP EFFECT ON AERODYNAMIC PERFORMANCE OF A FLAT PLATE WITH FORE AND AFT EMBEDDED ROTATING CYLINDERS

Hidayatullah Mohammad Ali [1,*] and Azmin Shakrine Mohd Rafie [1]

1. Department of Aerospace Engineering, Faculty of Engineering, Universiti Putra Malaysia, 43400 Serdang, Selangor, Malaysia.

*Correspondence: hidayatullah@upm.edu.my

Abstract: Boundary layer separation significantly affects aerodynamic performance of airfoils, turbine blades and flat plates, which reduces lift at high angles of attack and limits the efficiency in applications such as unmanned aerial vehicles (UAVs). A promising approach to delay the separation and enhance lift is the use of rotating cylinder near the surface, which leverages Magnus effect to inject momentum into the boundary layer. This study investigates the aerodynamic performance of a flat plate embedded with fore and aft rotating cylinder (CyFlaP), with particular emphasis on the influence of the gap size between the cylinders and the plate. The main objective is to identify the optimal gap configuration for maximizing lift coefficient (C_L) while ensuring flow stability across different Reynolds number regimes. Two-dimensional computational fluid dynamics (CFD) simulations were conducted in ANSYS Fluent, employing the SST k – ω turbulence model. For the analysis, the gap variation is from 1 mm to 10 mm while the inflow velocities ranging from 5 m/s to 30 m/s as these ranges capture the practical operating conditions and allow evaluation of their influence on the aerodynamic performance. A structured mesh with validated grid independence was used and the transient solver settings captured unsteady vortex dynamics around the rotating cylinders and flat plate. Results indicate that narrow gaps of 1 mm to 2 mm achieved the highest lift, with coefficients exceeding 3.7 at 20 degrees angle of attack for 5 m/s, corresponding up to 9% improvement over wider gaps. Nevertheless, this advantage diminished with increasing velocity, where wider gaps consistently underperformed and all configurations converged to C_L less than 1.4 at 25 m/s to 30 m/s. On the whole, the study concludes that gap tuning is most effective at low to moderate Reynolds numbers, with 1 mm identified as optimal and 2 mm to 3 mm offering a practical compromise for UAV applications. This effectiveness arises because smaller gaps enhance the momentum injection into the boundary layer, strengthening circulation around the plate and delaying flow separation while slightly larger gaps maintain lift enhancement without excessive viscous losses.

Keywords: boundary layer separation, computational fluid dynamics, gap variation, Magnus effect, unmanned aerial vehicle

1. Introduction

Boundary layer separation plays a critical role in determining aerodynamic performance in devices such as airfoils, turbine blades and flat plates [1]. At high angles of attack (α), flow separation over the upper surface reduces lift, leading to a lower lift coefficient (C_L) and impaired aerodynamic efficiency [2]. Delaying the separation of the boundary layer, which is the point where airflow detaches from the surface, is therefore essential, particularly in applications like unmanned aerial vehicles (UAVs) where maintaining attached flow helps to maximize lift without excessive weight or energy consumption. One effective method to enhance lift is momentum injection using a rotating cylinder near the surface of the body [3]. This mechanism is directly linked to the Magnus effect, in which a rotating body in a fluid

generates lift due to pressure differences around its surface [4]. The Magnus effect essentially provides the fundamental physical explanation for the lift benefits of rotating cylinders and is highly relevant for modern UAV designs.

In 1925, the application of a rotating cylinder embedment onto bluff geometry existed all the way back then [5]. The rotating cylinder embedment on the flat plate (CyFlaP) are influenced significantly by a past research work known as Leading Edge Cylinder Airfoil (LECA). In fact, the theory of LECA was first tested by Wolf [5] and Wolf and Koning [6] in 1925 and 1926, respectively, which resulted in enormous results for its aerodynamic performance. Till then, in 2014, Ahmed et al. [7] conducted a numerical analysis of a NACA 0024 airfoil with a rotating cylinder mounted at the leading edge using ANSYS CFX under the transient conditions and the SST turbulence model. Their study compared the modified airfoil with the baseline unmodified airfoil and reported that C_L of modified airfoil increased by 36% while its stall angle was delayed by 122%. This improvement in lift occurred because the rotating cylinder injected momentum into the boundary layer, strengthening circulation over the upper surface and delaying flow separation at higher angles of attack. The enhanced aerodynamic collectively indicates that leading edge cylinder rotation significantly improves the aerodynamic performance of the airfoil. Conversely, in 2015, Huda et al. [8] studied the LECA embedment onto NACA 0010 and produced the maximum model lift of 145% better than its unmodified model, thereafter delaying the separation flow at a higher momentum injection from the rotating cylinder. Moreover, recent research by Ali et al. [9] in 2021 demonstrated that CyFlaP could achieve up to a 76% increase in C_L compared to an unmodified flat plate. In 2022, Ali et al. [10] validated the concept on the Selig S1223 airfoil, showing that the dual rotating cylinders significantly delayed stall and improved lift at high angles of attack. Azman et al. [11] in 2022 extended this work further by developing a UAV prototype based on the CyFlaP design, which generated a lift force of 62.65 N at a velocity of 21 m/s and supported a payload of approximately 6.4 kN. While these studies confirmed the lift-generating potential, they also highlighted the importance of cylinder placement and rotation speed in maximizing lift performance.

A key parameter influencing lift in the CyFlaP system is the gap between the rotating cylinder and the flat plate. In 2017, Abdulla and Hasan [12] have numerically investigated on the effect of gap and found that the gap space of 3 mm was best for their study. They also denoted that the separation of the model at higher α did not appear as compared to the one without cylinder embedment. They concluded that the effect of gap has resulted with 35% and 21% better in lift and drag coefficients, respectively. The gap affects the momentum transferred into the boundary layer and subsequently the ability of the cylinder to control separation. Optimizing the gap is essential because an improperly sized gap could disturb the boundary layer, trigger premature flow separation and reduce the maximum achievable lift [13]. Modern computational studies allow systematic investigation of gap sizes, providing insights into how gap variation influences boundary layer behavior and lift generation. Further studies demonstrated that cylinder rotation speed and placement significantly affect the lift enhancement. Kamid et al. [14], Roslan et al. [15] and Zaimi et al. [16] have reported that higher rotational speed combined with optimal cylinder positioning suppress flow separation and stabilize unsteady flow structures, thereby increasing C_L. Additional bluff-body flow control strategies such as base bleed [17], top plate [18], end plates [19], splitter plates [20], secondary cylinders [21] and also sharp-edged flat tabs [22], have been explored to further improve lift and flow stability. However, unlike these auxiliary modifications, the gap in the CyFlaP configuration is an intrinsic design feature, hence its optimization is critical for the effective lift enhancement.

The CyFlaP flat plate also provides a controlled environment for examining the fundamental flow phenomena, including boundary layer behavior, vortex formation and unsteady wake structures. By systematically varying the gap size, it is possible to quantify how the momentum injection modifies the flow, delays separation and maximizes lift at different angles of attack. Insights from these analyses are highly relevant to the UAV design, where energy-efficient, lightweight and high-lift surfaces are essential for high-altitude operation. In this study, computational fluid dynamics (CFD) using ANSYS Fluent is

employed to perform two-dimensional simulations of CyFlaP configurations with the gap sizes ranging from 1 mm to 10 mm. The simulations aim to determine how the gap variation influences C_L and to identify optimal conditions for maximizing momentum transfer into the boundary layer. The findings provide a design guidance for high-lift UAV and contribute to a better understanding of unsteady flow dynamics in rotating-cylinder systems. By integrating the Magnus effect, CFD simulations and a detailed parametric analysis of gap size, this work seeks to enhance lift generation and provide practical insights for UAV and high-altitude platform design. The focus on gap optimization aligns the study with current technological needs and ensures relevance for both applied and fundamental aerodynamic research.

2. Methodology

The present study employs CFD to analyze the aerodynamic performance of a flat plate embedded with fore and aft rotating cylinders, with emphasis on the influence of gap variation. The computational procedure followed a structured approach, beginning with geometry generation, followed by turbulence model selection, mesh generation, solver configuration and validation through a mesh independency test. It can be noted that this methodology has been widely adopted in prior aerodynamic investigations to ensure reliability and reproducibility of CFD results [23].

2.1 Geometry configurations

The rotating cylinders form the foundation of CyFlaP configuration. Badalamenti [24] investigated the aerodynamic performance using wind tunnel testing at City University's Handley Page Aerodynamic Laboratory, validating the effects of cylinder rotation on flow control. The experimental results were consistent with Betz's theoretical work, which identified an aspect ratio (AR) of 4.7 as significant for the aerodynamic scaling [25]. For this study, the cylinder dimension follows Badalamenti's configuration with an applied AR of 5.1. Each cylinder has a diameter of 0.16 m and is rotated clockwise, consistent with Badalamenti [24]. Clockwise rotation accelerated the flow above the cylinder and decelerated it below, thereby generating an upward Magnus lift force as noted by Barati et al. [26]. The schematic of the rotating cylinder is shown in Figure 1.

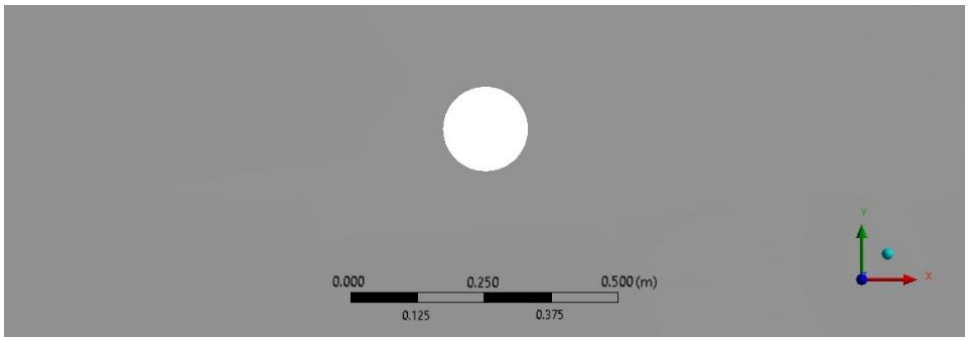

Figure 1: Rotating cylinder schematic diagram

The flat plate serves as the baseline aerodynamic surface onto which the cylinders are embedded. Its aerodynamic simplicity and effectiveness have been highlighted by Wang et al. [27] and Torres and Mueller [28], who demonstrated that flat plates can sustain high α, achieving up to 60% of the maximum lift coefficient (C_{Lmax}) of conventional airfoils. For this study, the flat plate has a chord length of 1 m. The schematic of the flat plate baseline is shown in Figure 2.

The combined CyFlaP configuration was first proposed by Modi [29], originally to reduce drag in bluff bodies such as trucks. In Modi's early work, the rotating cylinders were mounted close to the

bluff-body surfaces primarily for drag reduction, but the exact gap between the cylinder and surface was not systematically varied or optimized as the configuration emphasized the qualitative flow control rather than the parametric gap studies. Later studies extended its application to the lift enhancement by embedding rotating cylinders along the camber line of the flat plate. In this arrangement, cylinders are positioned at the leading edge and trailing edges with a defined separation gap from the plate surface. Abdulla and Hasan [12] demonstrated that the gap strongly influences aerodynamic performance, with intermediate values yielding optimal lift-to-drag ratios. Specifically, Abdulla and Hasan [12] investigated gap sizes of 1 mm, 2 mm, 3 mm, 4 mm and 5 mm for embedded rotating cylinder at the leading edge of a NACA 0012 airfoil and identified the 3 mm gap as the optimum configuration across velocity ratios (U_C/U_∞ = 1 to 3). In this study, the gap sizes ranging from 1 mm to 10 mm are investigated to examine their effect on the momentum injection, separation delay and lift augmentation. Thus, the current work expands the explored parameter space by testing gaps up to 10 mm, considerably wider than the 1 mm to 5 mm range studied by Abdulla and Hasan [12], and by applying the CyFlaP concept to a flat plate configuration rather than the NACA 0012 airfoil geometry used previously. The CyFlaP geometry with embedded cylinders and gap variation is illustrated in Figure 3.

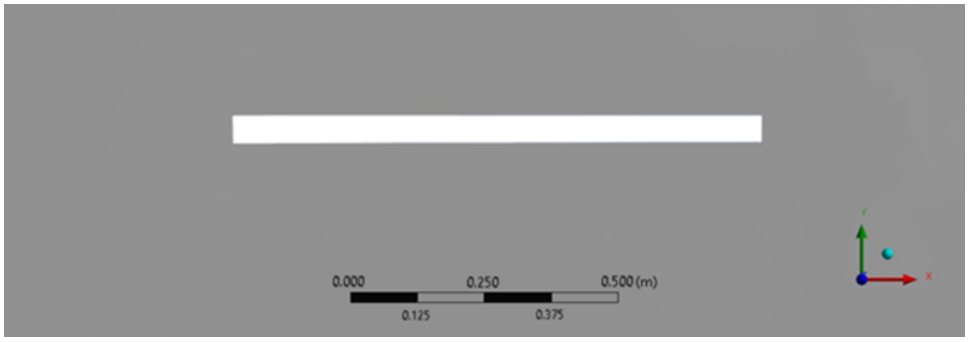

Figure 2: Flat plate schematic diagram

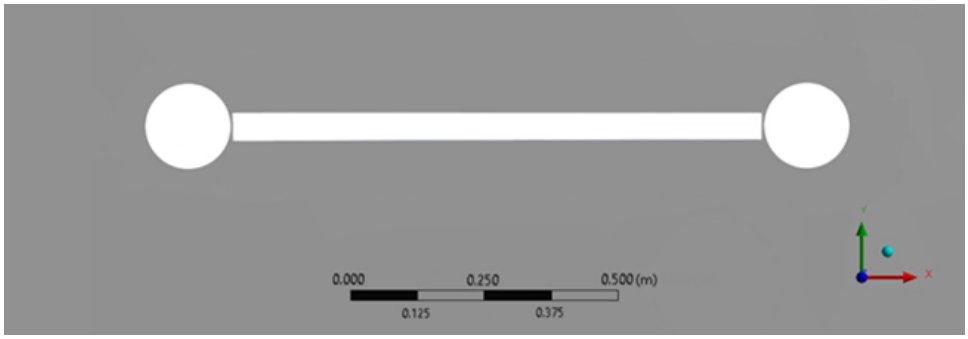

Figure 3: CyFlaP geometry with embedded cylinders and gap variation schematic diagram

2.2 Turbulence model

In general, the turbulence modelling provides a numerical approach to close the Reynolds-averaged Navier-Stokes (RANS) equations, enabling prediction of the turbulent flow effects through additional transport equations. In this study, the Shear Stress Transport (SST) k – ω model was selected, following its successful application in similar aerodynamic investigations by Ali et al. [9, 30] and Mgaidi et al. [31]. The two-equation model introduces the turbulent kinetic energy (k) as the first transported variable and the specific dissipation rate (ω) as the second variable, allowing accurate presentation of the turbulent transport properties.

The SST k – ω model was introduced by Menter [32] as improvement over Wilcox's original k – ω formulation [33]. Its formulation blends the advantages of the k – ω model in the near-wall region with the k – ω model in the far field, thereby reducing sensitivity to free-stream turbulence levels. This hybrid approach enhances predictive accuracy in flows with strong adverse pressure gradients and separation, which are central features of the CyFlaP configuration. The transport equations for the SST k – ω model are expressed as in Equation 1 and Equation 2.

$$\frac{\partial}{\partial t}(\rho k) + \frac{\partial}{\partial x_i}(\rho k u_i) = \frac{\partial}{\partial x_j}\left[\Gamma_k \frac{\partial k}{\partial x_j}\right] + G_k - Y_k + S_k \quad (1)$$

$$\frac{\partial}{\partial t}(\rho \omega) + \frac{\partial}{\partial x_i}(\rho \omega u_i) = \frac{\partial}{\partial x_j}\left[\Gamma_\omega \frac{\partial \omega}{\partial x_j}\right] + G_\omega - Y_\omega + S_\omega \quad (2)$$

Equation 1, which is transport equation for k, describes how turbulence is produced, transported and dissipated in the flow. In this equation, G_K represents the generation of turbulent kinetic energy due to mean velocity gradients, indicating how shear in the flow produces turbulence. Y_K denotes the dissipation of k into thermal energy due to viscous effects while Γ_K represents the effective diffusivity controlling the spatial transport of k. An additional source term, S_K allows user-defined contributions to turbulent kinetic energy if necessary. Similarly, the transport equation for ω in Equation 2 describes how the turbulence decay rate evolves in the flow. In this equation, G_ω represents the generation of ω due to the velocity gradients, Y_ω is the dissipation of ω and Γ_ω is the effective diffusivity controlling its transport. S_ω accounts for any user-defined sources for ω. Together, Equation 1 and Equation 2 provide a complete description of the production, diffusion, and dissipation of turbulence in the flow, allowing the SST k – ω model to accurately capture the near-wall behavior, flow separation, and unsteady vortical structures in the CyFlaP configuration.

2.3 Grid generation and mesh validation

The pre-processing stage of this research required the construction of a computational grid that properly defined the boundaries and ensured reliable two-dimensional (2D) numerical simulations. In CFD, grid generation is one of the most crucial steps as the accuracy of the numerical solution depends heavily on the mesh quality and the suitability of its configuration for capturing the governing Navier-Stokes equations. In line with the approaches of Mgaidi et al. [31] and Yao et al. [34], a block-structured mesh was adopted for this study to balance the computational efficiency with the solution fidelity. The computational domain was established using a double rectangular block arrangement, consisting of an inner block of 2D x 3D surrounding the model and an outer block of 6D x 15D extending further into the far-field as shown in Figure 4(a). Here, D denotes the diameter of the rotating cylinder, which serves as the reference length for domain scaling. To adequately capture near-wall effects, inflation layers were applied on the model surfaces, consisting of 15 layers with a growth rate of 1.2, ensuring a y-plus (y^+) value of less than 1 as shown in Figures 4(b) and 4(c). This configuration provided sufficient resolution of the boundary layer and allowed for consistent implementation of the wall function approach under the selected turbulence model.

In this study, wall functions were employed with the SST k – ω model to ensure numerical stability and to reduce excessive grid requirements, particularly in regions where strong curvature and cylinder rotation-generated shear could otherwise demand extremely fine near-wall resolution. The use of wall functions therefore enabled a practical balance between computational cost and accuracy. The standard automatic wall treatment provided in the solver, which switches between the low-Reynolds-number integration and wall functions depending on local y^+, was used to accommodate the fine mesh near the

rotating cylinder while maintaining robust convergence in the far-field and less sensitive regions. The boundary conditions and mesh parameters employed in the setup are tabulated in Table 1 and Table 2.

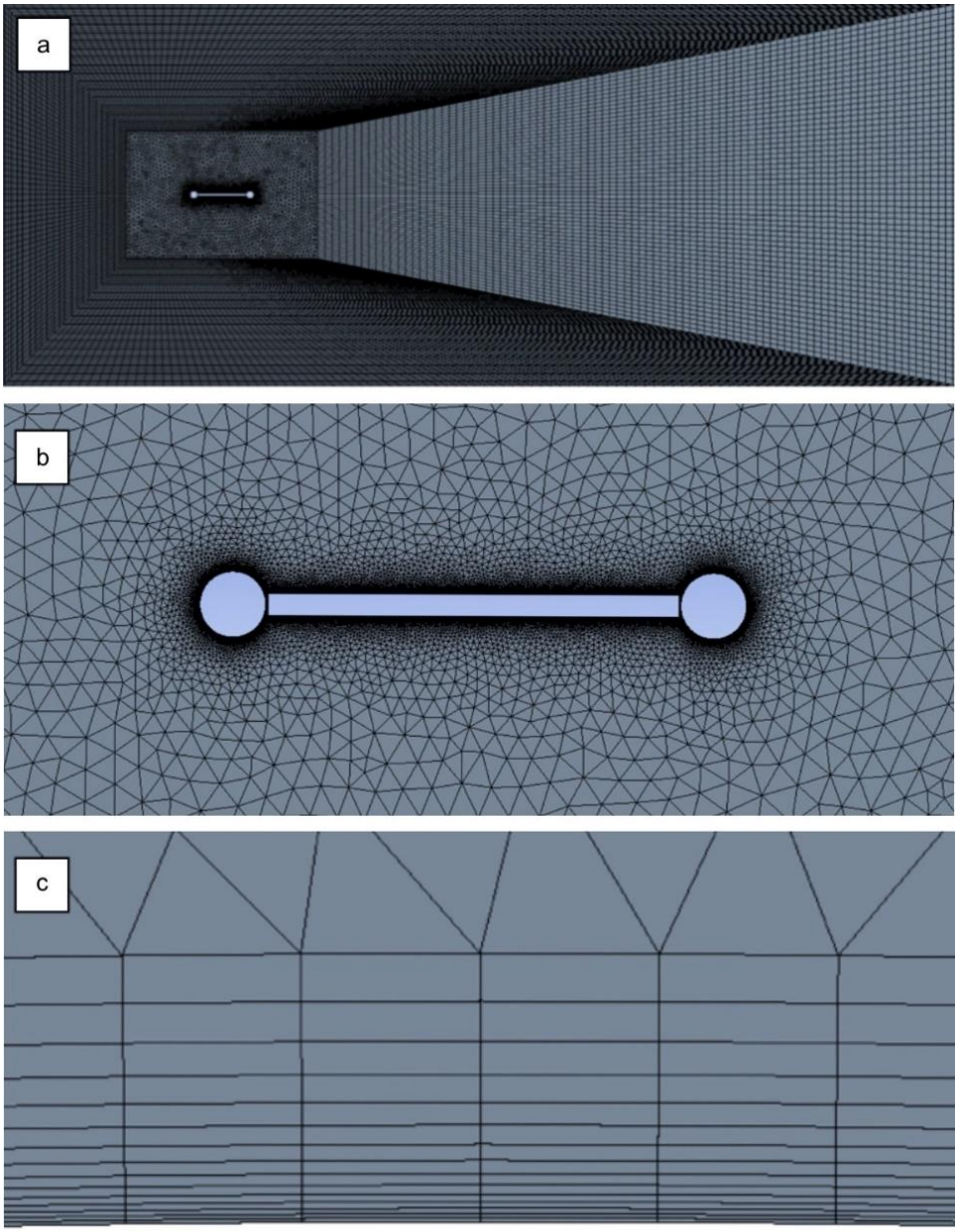

Figure 4: CyFlaP's computational setup showing: (a) domain configuration, (b) mesh generation near the model, (c) surface-body inflation layers

Table 1: Boundary conditions

Boundary conditions	**Type**
Inlet	Velocity-inlet
Outlet	Pressure-outlet
Cylinder	Wall
Selig airfoil	Wall
Wall	Symmetry
Interior surface body	Interior
Surface body	Interior

Table 2: Mesh setups

Mesh specifications	
Growth rate	1.2
Defeature size	5.e-004 m
Curvature minimum size	1.e-003 m
Curvature normal angle	18.0°
Smoothing	High
Inflation specifications	
Inflation option	First layer thickness
Maximum layers	15
Growth rate	1.2

The boundary condition strategy in this study followed the standard aerodynamic practice to ensure a realistic flow modelling. A velocity-inlet was specified at the upstream boundary to define the inflow velocity while pressure-outlet at the downstream boundary allowed smooth outflow without reflections. The cylinder and airfoil walls were treated as no-slip conditions to capture the viscous effects, with a symmetry boundary at the far-field wall to represent an unbounded domain. The interior surfaces were assigned as "Interior" to facilitate continuity between grid regions. The mesh specifications, including a growth rate of 1.2, defeature size of 5 x 10^{-4} m, curvature minimum size of 1 x 10^{-3} m and also high smoothing, were selected to maintain the accuracy in curved regions while ensuring overall numerical stability.

Before proceeding with the solver settings, a mesh independency test was performed to confirm the reliability of the grid and ensure solution independence from mesh density. Following the approach of Ali et al. [9] and Yao et al. [34], successive refinement of the grid was tested for both the rotating cylinder and the flat plate embedment configurations as depicted in Figure 5 and Figure 6, respectively. Two iterations of the mesh independency test were carried out and convergence of the C_L was observed at approximately 4.19 x 10^4 cells for the rotating cylinder and 9.19 x 10^4 cells for the flat plate. At these refinement levels, the error percentage fell below 1%, which confirmed that the selected mesh was both computationally efficient and also sufficiently accurate for capturing the required flow physics. This validated mesh configuration was therefore adopted for the subsequent CFD simulations.

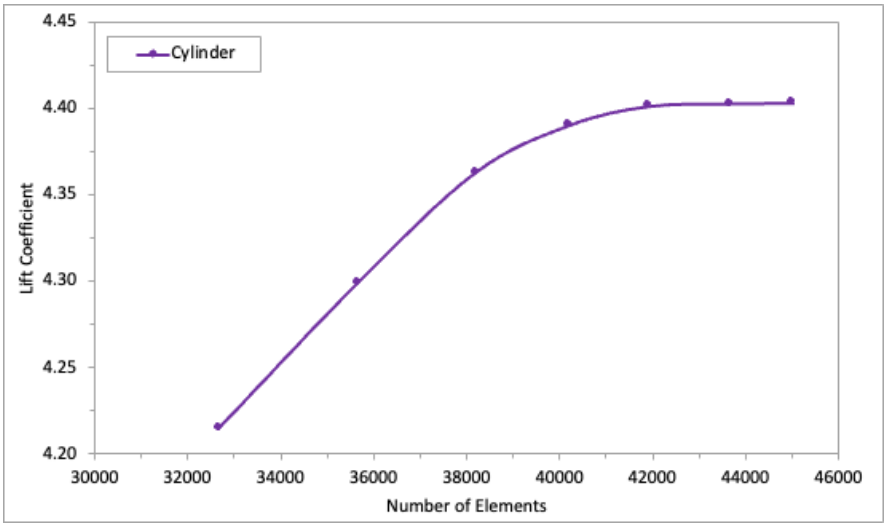

Figure 5: Cylinder's mesh independency test results

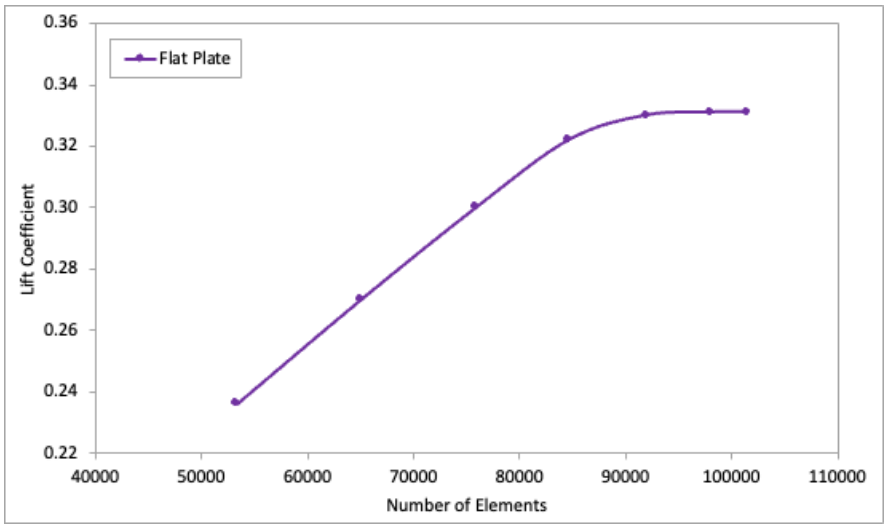

Figure 6: Flat plate's mesh independency test results

2.4 Solver setup

The numerical solution process relies heavily on the solver configuration, as it governs both the accuracy of the predictions and the stability of convergence. In this study, a pressure-based formulation was adopted, consistent with the incompressible and subsonic flow conditions of interest. A transient framework was employed to resolve the unsteady nature of the vortex shedding and the time-dependent interactions around the rotating cylinder and flat plate, which the steady-state models cannot adequately capture. To model the turbulence, the SST k – ω approach was applied, offering robust performance in resolving boundary-layer behaviour while retaining stability in the free-stream. This hybrid formulation is particularly effective for flows where separation and near-wall stresses play the decisive role in the aerodynamic performance. Reference values such as density, viscosity and freestream velocity were specified under the standard atmospheric conditions to ensure the physical consistency in evaluating aerodynamic characteristics across a range of operating speeds. The solution strategy employed coupled pressure-velocity iteration, a method that enhances the convergence reliability in flows with strong momentum-pressure interactions as in the case of rotating bodies. A stringent residual convergence criterion of 10^{-6} was enforced to maintain the solution fidelity throughout the computational domain. Spatial discretization schemes were selected to minimise numerical diffusion while preserving accuracy in regions with steep gradients.

The PRESTO! Algorithm was applied for pressure interpolation, offering superior resolution in swirling and rotational flows, while the QUICK scheme was used for momentum, turbulent kinetic energy and specific dissipation rate equations to capture the convection-dominated transport without excessive artificial smoothing. Gradient calculations relied on the Green-Gauss node-based method, ensuring a sharp resolution at interfaces and curved surfaces. Together, the solver setting provided a balance of computational efficiency and predictive accuracy, tailored to capture the complex unsteady aerodynamics central to this investigation.

2.5 Validation

A validation study was conducted for both the rotating cylinder and the flat plate prior to advancing with the CFD simulations as illustrated in Figure 7 and Figure 8, respectively. Particular attention was given to the embedding of these geometries within the computational domain to ensure the consistency with experimental configurations. The experimental investigations reported by Badalamenti and Prince

[24] and Torres and Mueller [28] provided the reference data for comparison, against which the present CFD results were assessed. The validation demonstrated good agreement, with discrepancies remaining within 10%, thereby confirming the reliability of the numerical setup for subsequent analysis.

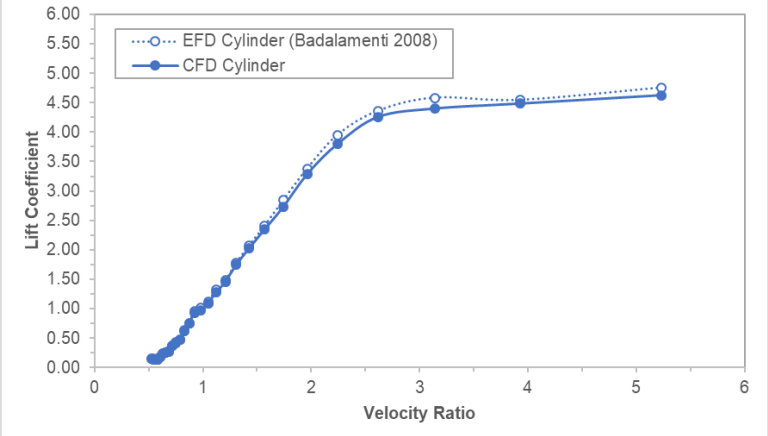

Figure 7: Cylinder's validation results

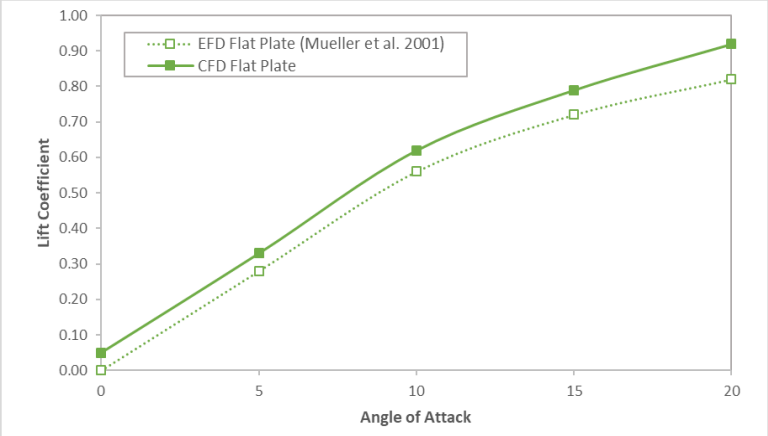

Figure 8: Flat plate's validation results

3. Results and Discussion

The aerodynamic behavior of the CyFlaP configuration was further examined by analyzing the C_L variations across a range of free-stream velocities, gap sizes and velocity ratios (V_r). The dataset was systematically organized into six sets, corresponding to the inflow velocities of 5, 10, 15, 20, 25 and 30 m/s. Within each velocity set, the effect of the gap size, ranging from 1 mm to 10 mm, was evaluated against V_r values from 0 to 20. This approach enables a detailed understanding of how flow separation, circulation and interaction between the cylinder and flat plate evolve within changing geometric spacing and dynamic conditions. By comparing these results, quantitative trends can be highlighted, identifying the gap configurations and operating conditions that maximize aerodynamic performance.

At free-stream velocity of 5 m/s, corresponding to Reynolds number of 456,140, the C_L showed a consistent upward trend with increasing angle of attack for all gap sizes between 1 mm and 10 mm, as shown in Figure 9. At zero degrees, C_L values ranged from 2.39 at 10 mm to 2.97 at 2 mm, indicating that smaller gaps promoted a stronger lift generation at low incidence. As the angle of attack increased

to 20 degrees, C_L peaked between 3.55 at 10 mm and 3.88 at 2 mm, reinforcing the dominance to tighter gap spacing in sustaining circulation and delaying flow separation.

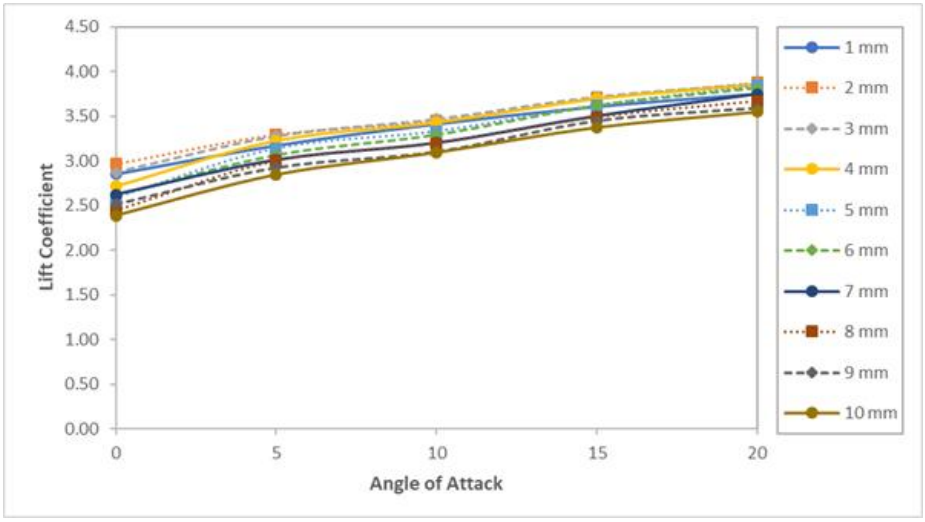

Figure 9: Lift coefficient versus angle of attack for different gap variations at 5 m/s

The C_L difference across gap sizes at 20 degrees was approximately 0.33, which is significant given the relatively low inflow velocity. Interestingly, progression of C_L with angle of attack remained smooth across all gaps, with no evident deterioration in lift even at higher incidence angles. This suggests that at low Reynolds number, the gap effect plays a stabilizing role, particularly for smaller separations, as the CyFlaP system benefits from enhanced interaction of the boundary layers. Overall, the 5 m/s results indicate that narrow gaps, especially between 2 mm and 3 mm, give the most favorable lift performance, offering nearly 9% improvement in C_L compared to wider separations. The improvement arises because tighter gaps enhance the interaction between boundary layers on the adjacent surfaces, strengthening circulation and delaying flow separation. Physically, smaller gaps constrain the flow between the rotating cylinder and the flat plate, increases the shear and accelerates the gap-flow generated by the cylinder's surface motion. This accelerated near-wall flow will increase the local velocity over the leading edge, deepening the suction peak and thereby enhancing the circulation, consistent with the Kutta-Joukowski relation [35]. A reduced gap also limits the cross-flow entrainment and helps maintain a more coherent attached boundary layer, delaying separation and improving the effective turning of the flow around the plate. Prior studies, including Abdulla and Hasan [12], have reported that the optimum lift occurs at intermediate gap sizes because larger gaps weaken the cylinder-induced momentum transfer while excessively small gaps can inhibit flow entrainment or cause adverse pressure buildup. Consequently, C_L peaks at smaller gaps such as 2 mm to 3 mm, where the coupling between the rotating cylinder and the plate is strongest, maximizing the momentum transfer and producing the most favorable pressure distribution for lift generation. As a result, the system sustains higher lift even at larger angles of attack, highlighting the critical role of gap spacing in optimizing the aerodynamic performance at low Reynolds numbers.

At the free-stream velocity of 10 m/s, corresponding to a Reynolds number of 912,279, the gap-dependent trends in lift coefficient became more distinct compared to that of the 5 m/s case as shown in Figure 10. At zero degree, the 1 mm gap recorded a C_L of 2.13, slightly lower than the 2.86 achieved at 5 m/s, suggesting that higher velocities reduced the baseline lift across all gaps. Nonetheless, the narrow gaps maintained a relative advantage, with C_L gradually increasing with angle of attack to reach 2.79 at 20 degrees for the 1 mm case. In contrast, the wider 10 mm gap yielded lower lift levels, from 1.29 at zero degree to 2.51 at 20 degrees, highlighting a widening disparity between narrow and wide spacing as Reynolds number increased. Unlike the smoother progression seen at 5 m/s, the lift response

here began to show signs of sensitivity to angle of attack, particularly at intermediate gaps such as 4 mm and 5 mm, where C_L values increased steadily up to 20 degrees without a clear plateau or dip. This indicates that, at 10 m/s, flow attachment near the cylinder to flat plate interface was less stable, with separation effects more evident for mid- to wide-gap configurations. Taken together, the results show that although the general hierarchy of performance for the narrow gaps outperforming wider ones while remains intact, the degree of lift augmentation diminishes compared to the lower velocity conditions, marking an early shift toward Reynolds-number-driven flow dynamics.

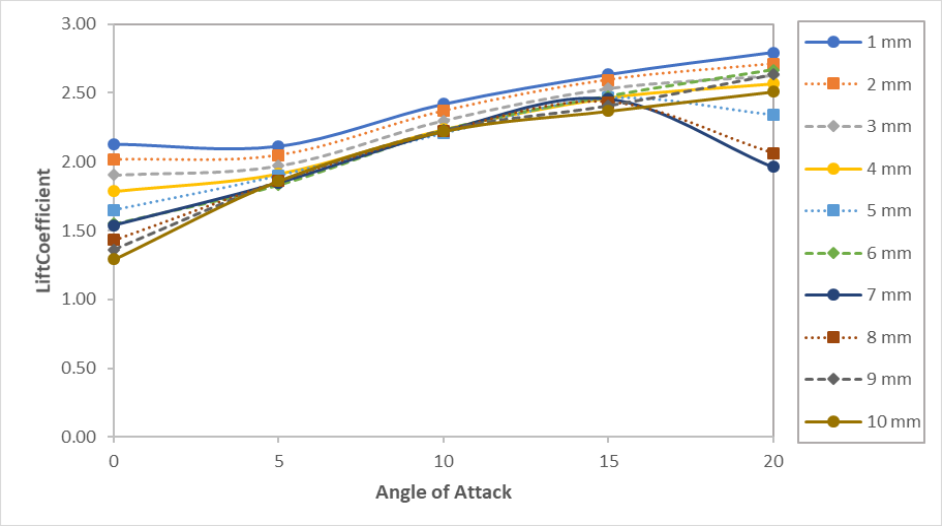

Figure 10: Lift coefficient versus angle of attack for different gap variations at 10 m/s

At 15 m/s, corresponding to Reynolds number of 1,368,419, the relationship between gap spacing and lift coefficient became increasingly nuanced. For 1 mm gap, the C_L initiated at 1.67 at zero degree and climbed steadily to 3.15 at 20 degrees. While still higher than wider-gap configurations, these values were notably lower than those recorded at 10 m/s, confirming that lift generation efficiency weakens as velocity and Reynolds number increase. Wider gaps continued to trail behind for the 10 mm spacing, producing a C_L of 0.93 at zero degree to 1.69 at 20 degrees, widening the disparity between narrow and wide configurations. Intermediate gaps such as 5 mm and 6 mm showed more modest gains, reaching only 1.82 and 1.64 respectively at 20 degrees, underscoring their weaker capacity to sustain circulation compared to the narrow gaps. Unlike the smoother growth patterns evident at lower velocities, the 15 m/s results revealed some irregularities in the lift response, particularly among mid-gap cases where the increments diminished beyond 15 degrees and in some cases hinted at minor reductions. This behavior points to earlier onset of the flow separation and weakened vortex interactions in higher-Re conditions, where the stabilizing influence of narrow gaps became more critical. Overall, Figure 11 underscores a transition although narrow gaps still dominate, the relative gains diminish with rising Reynolds number, suggesting that geometric optimization becomes less influential as inertial effects grow stronger.

At free-stream velocity of 20 m/s, which was corresponding to Reynolds number of 1,824,558, the diminishing benefits of gap optimization became more evident. For 1 mm gap, the C_L started at 1.33 at zero degree and increased steadily to 2.87 at 20 degrees. Although this remained as the highest among all gaps, the improvement beyond 15 degrees was modest compared to lower velocities, reflecting the growing influence of the inertial effects. Wider gaps continued to lag behind, for instance, the 10 mm spacing produced only 0.77 at zero degree and 1.43 at 20 degrees, widening the disparity between the narrow and the wide configurations. Intermediate gaps displayed irregular trends. The 4 mm case, for example, climbed to 1.54 at 10 degrees, dipped slightly to 1.40 at 15 degrees, and then rose sharply to 2.46 at 20 degrees, highlighting unstable flow reattachment dynamics. Unlike smooth and monotonic

increases observed at 5 m/s and 10 m/s, the lift curves at this Reynolds number revealed plateaus and abrupt fluctuations, which were characteristic of stronger separation effects. Overall, while narrow gaps still dominate in performance, the relative advantage as shown in Figure 12 diminishes at this higher velocity, signaling a transition toward Reynolds-number-driven flow behavior.

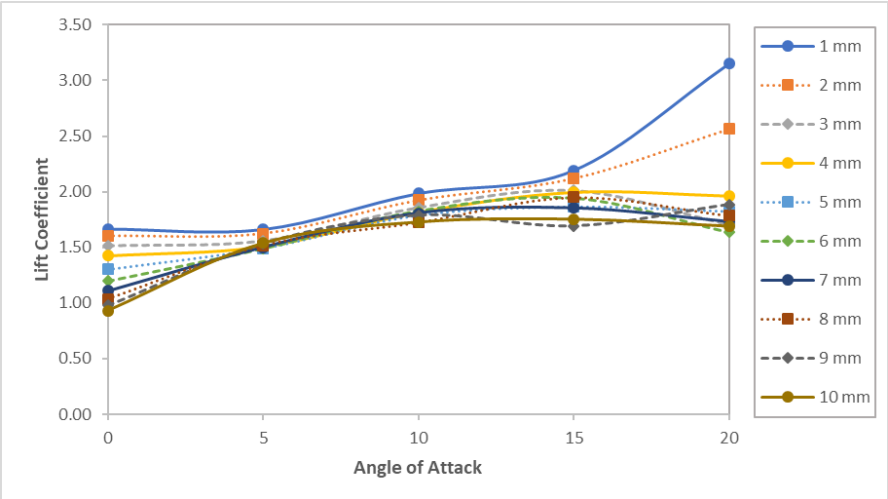

Figure 11: Lift coefficient versus angle of attack for different gap variations at 15 m/s

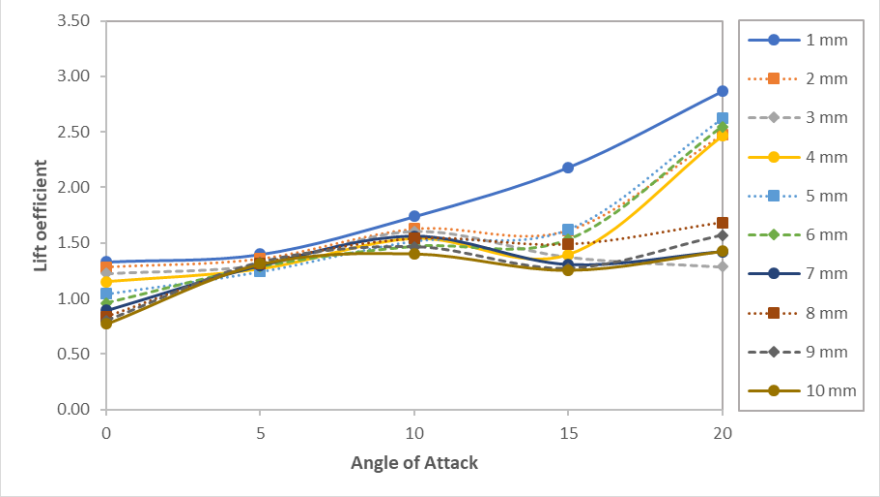

Figure 12: Lift coefficient versus angle of attack for different gap variations at 20 m/s

At 25 m/s, with Reynolds number of 2,280,698, the overall lift levels further continued to decline, underscoring the weakening effect of gap tuning at higher flow speeds. The narrow 1 mm gap, once clearly dominant, produced only 1.40 at 20 degrees, a sharp drop from 2.87 at the same angle in the 20 m/s case. Wider gaps converged toward similarly modest values, with the 10 mm gap delivering 1.24 at 20 degrees. The mid-gap configurations showed more erratic behavior with the 5 mm case climbed gradually to 1.52 at 15 degrees before jumping unexpectedly to 2.62 at 20 degrees, while the 4 mm gap followed a similar surge, reaching 2.07 at 20 degrees. These late peaks suggest that separation-induced reattachment becomes highly unsteady at this velocity, occasionally boosting lift but in an unpredictable fashion. Therefore, the trend at 25 m/s as shown in Figure 13 is one of signals that stability rather than peak lift may be the more relevant metric at this regime.

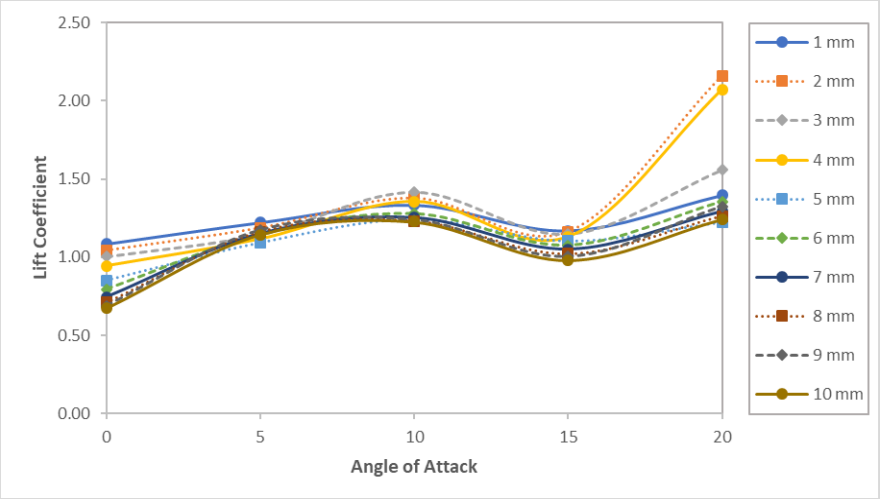

Figure 13: Lift coefficient versus angle of attack for different gap variations at 25 m/s

At 30 m/s, corresponding to Reynolds number of 2,736,838, the lift curves had flattened almost completely, showing that the inertial dominance largely overwhelms the gap-related effects. Across all configurations, C_L values clustered tightly between 0.8 and 1.4 at zero incidence and rarely exceeded 1.37 at 20 degrees as shown in Figure 14. The 1 mm gap, though still nominally ahead with a peak of 1.28 at 20 degrees, no longer exhibited the clear superiority seen at lower speeds. Mid-gap spacing such as 5 mm and 6 mm hovered around 1.35 at best while the widest 10 mm gap barely reached 1.06 at 20 degrees. The uniformity of these outcomes suggests that the system has entered a separation-dominated state in which the boundary-layer interactions contribute little to lift augmentation. In this regime, the optimization of narrow gaps provides only marginal benefits, and the performance hierarchy collapses into a narrow band of diminished effectiveness.

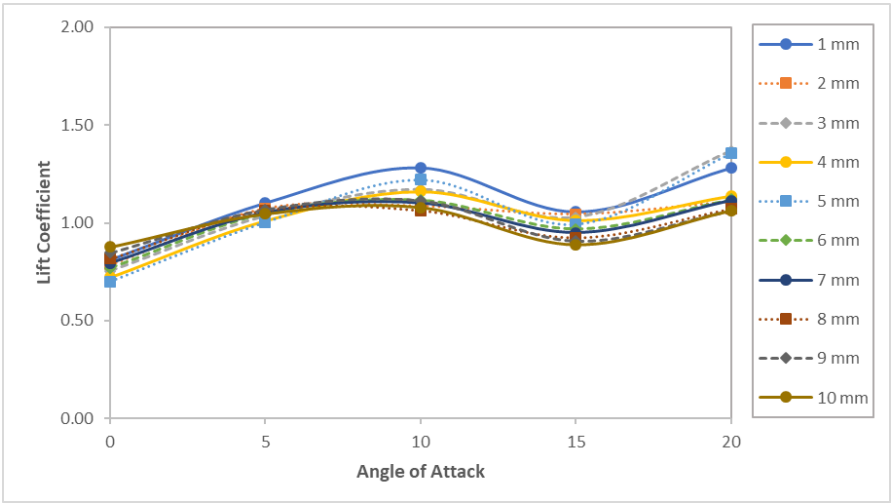

Figure 14: Lift coefficient versus angle of attack for different gap variations at 30 m/s

Across all examined velocities from 5 to 30 m/s, the results demonstrate that gap spacing exerts its strongest influence at low Reynolds numbers where the narrow separations between 1 mm to 2 mm consistently produced the highest C_L, exceeding 3.7 at 20 degrees in 5 m/s case. As velocity increased, the advantage of the small gaps diminished steadily, with intermediate configurations showing irregular patterns and wide gaps offering consistently weaker performance. By 25 m/s and 30 m/s, the lift values

had collapsed into a narrow range regardless of the spacing, confirming that the inertial and separation-dominated flow mechanisms ultimately suppress the benefits of the geometric optimizations. Taken together, the findings establish that the gap tuning is most effective in the low to moderate Reynolds number regimes while at higher flow speeds, its influence becomes marginal.

4. Conclusion

This study has examined the aerodynamic performance of the CyFlaP system across a range of gap spacing and free-stream velocities, with emphasis on the lift enhancement achievable through geometric tuning. The results have shown that at low velocities of 5 m/s to 10 m/s, corresponding to Reynolds numbers below one million, narrow gaps of 1 mm to 2 mm delivered the most favorable performance, achieving C_L in excess of 3.7 at 20 degrees. These conditions demonstrated stable lift growth with angle of attack and confirmed that close interaction between the cylinder and the flat plate promotes a strong circulation and delayed separation. As the velocity increased toward 15 m/s and 20 m/s, the absolute lift levels declined and irregularities emerged for intermediate gaps, reflecting earlier onset of separation and weakening of vortex interactions. Wider gaps of 8 mm to 10 mm consistently produced inferior performance, often yielding C_L below 1.5 at higher angles. At highest velocities of 25 m/s and 30 m/s, the overall lift performance converged across all gap sizes, with the values of C_L rarely exceeding 1.4, underscoring the dominance of inertial effects and the diminishing role of geometry in shaping flow behavior. Although the 1 mm gap was identified as the optimal configuration throughout, its practical implementation may be limited by manufacturing tolerances and operational constraints. As such, gaps of 2 mm to 3 mm present a more realistic compromise, offering substantial lift enhancement while maintaining greater feasibility in design and application. Future work may extend this analysis to include unsteady flow effects, structural considerations and three-dimensional configurations to further assess the aerodynamic potential of the CyFlaP concept.

Acknowledgement

This work was supported by the Malaysian Ministry of Education under Fundamental Research Grant Scheme (FRGS/1/2018/TK09/UPM/02/2). The author would also like to thank the Faculty of Engineering, Universiti Putra Malaysia for providing the computational facilities.

References

[1] J. Svorcan, J. M. Wang and K. P. Griffin, 'Current State and Future Trends in Boundary Layer Control on Lifting Surfaces', Advances in Mechanical Engineering, vol. 14, no. 7, 2022.

[2] M. Simons, Model Aircraft Aerodynamics. Fox Chapel Publishing, 2025.

[3] S. Abdolahipour, 'Review on Flow Separation Control: Effects of Excitation Frequency and Momentum Coefficient', Frontiers in Mechanical Engineering, vol. 10, p. 1380675, 2024.

[4] M. H. Al Faruq, S. I. Pranto, M. Kasfia, J. H. Samin, M. F. Chhoa, A. S. Jahin and H. I. Nokib. (2024). Exploring Magnus Effect: A Review of Its Influence on Airfoil Performance and Industrial Applications [Online]. Retrieved from https://doi.org/10.2139/ssrn.4935291

[5] E. Wolff. (1925). Preliminary Investigation of the Effect of a Rotating Cylinder in a Wing [Online]. Retrieved from https://digital.library.unt.edu/ark:/67531/metadc59069/

[6] E. Wolff and C. Koning. (1926). Tests for Determining the Effect of a Rotating Cylinder Fitted into the Leading Edge of an Airplane Wing [Online]. Retrieved from https://digital.library.unt.edu/ark:/67531/metadc65163/

[7] S. Ahmed, A. Nazari and E. Wahba, 'Numerical Analysis of Separation Control Over an Airfoil Section', International Review of Aerospace Engineering, vol. 7, no. 2, pp. 61-68, 2014.

[8] M. N. Huda, T. Ahmed, S. S. Ahmed and M. A. Salam, 'Study of NACA 0010 Symmetric Airfoil with Leading Edge Rotating Cylinder in a Subsonic Wind Tunnel', Proceedings of the 11th International Conference on Mechanical Engineering, Dhaka, Bangladesh, December 2015.

[9] H. M. Ali, A. S. M. Rafie, S. A. M. Ali and E. Gires, 'Computational Analysis of the Rotating Cylinder Embedment onto Flat Plate', CFD Letters, vol. 13, no. 12, pp. 133-149, 2021.

[10] H. M. Ali, A. S. M. Rafie, M. Hamid and S. Ali, 'Comparative Computational Study of Double Rotating Cylinder Embedded on Selig S1223 Aerofoil and Flat Plate for High Altitude Platform', Pertanika Journal of Science and Technology, vol. 30, pp. 2767-2788, 2022.

[11] S. W. Azman, A. S. M. Rafie and E. Gires, 'Aerodynamic Analysis of Cylinder to Flat Plate (CyFlap) Embedment for Agriculture Purposes', Journal of Aeronautics, Astronautics and Aviation, vol. 56, no. 1S, pp. 357-364, 2024.

[12] N. N. Abdulla and M. F. Hasan, 'Effect of Gap between Airfoil and Embedded Rotating Cylinder on the Airfoil Aerodynamic Performance', Research & Development in Material Science, vol. 3, no. 4, 2018.

[13] F. Z. Wang, I. Animasaun, T. Muhammad and S. Okoya, 'Recent Advancements in Fluid Dynamics: Drag Reduction, Lift Generation, Computational Fluid Dynamics, Turbulence Modelling and Multiphase Flow', Arabian Journal for Science and Engineering, vol. 49, no. 8, pp. 10237-10249, 2024.

[14] M. I. Kamid, H. M. Ali and A. S. M. Rafie, 'Computational Aerodynamics Analysis of a Bluff Body with Rotating Cylinder as Drag Reducer', Journal of Aerospace Society Malaysia, vol. 1, no. 1, pp. 34-45, 2023.

[15] M. S. I. Roslan, H. M. Ali and A. S. M. Rafie, 'Rotational Speed Analysis on Double Rotating Cylinder for Cylinder to Flat Plate using Numerical Method', Journal of Aeronautics, Astronautics and Aviation, vol. 55, no. 3S, pp. 495-506, 2023.

[16] U. Z. Zaimi, H. M. Ali and A. S. M. Rafie, 'Experimental Analysis on Pitching Moment for Embedment Cylinder to Flat Plate High Altitude Platform Station', in International Seminar on Aeronautics and Energy, Springer, 2022.

[17] M. A. Akar and H. Akıllı, 'Base Bleed Flow Control Tool for Circular Cylinders with Three Side-By-Side Arrangements in Shallow Water', International Journal of Pioneering Technology and Engineering, vol. 2, no. 01, pp. 128-134, 2023.

[18] H. M. Ali, A. S. M. Rafie, M. F. A. Hamid and S. A. M. Ali, 'Concentrated Flow Effects on Aerodynamics Performance for CyFlaP Magnus UAV by using Computational Approach', CFD Letters, vol. 18, no. 3, pp. 134-151, 2025.

[19] J. Liu, W. Ma, D. Zheng, L. Jin and Q. Liu, 'Numerical Investigation of Cylinder Rotors with Various Endplates', Physics of Fluids, vol. 36, no. 7, 2024.

[20] H. Zhu, T. Tang, M. M. Alam, J. Song and T. Zhou, 'Flow-induced Rotation of a Circular Cylinder with a Detached Splitter Plate and Its Bifurcation Behavior', Applied Ocean Research, vol. 122, p. 103150, 2022.

[21] Y. Zhang and Y. Zhao, 'Novel Design of a Circulation Control Airfoil with Cylinder Rotation', Physics of Fluids, vol. 35, no. 8, 2023.

[22] A. Boral, S. Dutta, A. Das, A. Kumar, N. Bej, P. Chaubdar, B. N. Das and A. B. Harichandan, 'Drag Reduction for Flow Past Circular Cylinder using Static Extended Trailing Edge', ASME Open Journal of Engineering, vol. 2, p. 021016, 2023.

[23] K. Subramaniam and W. S.-I. W. Salim, 'A Review of Experimental Approaches for Investigating the Aerodynamic Performance of Drones and Multicopters', Journal of Advanced Research in Experimental Fluid Mechanics and Heat Transfer, vol. 14, no. 1, pp. 1-24, 2023.

[24] C. Badalamenti and S. Prince, 'Effects of Endplates on a Rotating Cylinder in Crossflow', Proceedings of 26th AIAA Applied Aerodynamics Conference, Honolulu, USA, August 2008.

[25] A. Betz, 'Der magnuseffekt, die grundlage der flettner—walze', Zeitschrift des vereins deutscher Ingenieure. Translated to: The "Magnus Effect" The Principle of the Flettner Rotor. NACA Technical Memorandum, TM-310, pp. 9-14, 1925.

[26] E. Barati, M. R. Zarkak and J. A. Esfahani, 'Effect of Rotational Direction of Circular Cylinder for Mixed Convection at Subcritical Reynolds Number', Proceedings of the 27th Annual International Conference of Iranian Society of Mechanical Engineers, Tehran, Iran, April-May 2019.

[27] S. Wang, X. Zhang, G. He and T. Liu, 'A Lift Formula Applied to Low-Reynolds-Number Unsteady Flows', Physics of Fluids, vol. 25, no. 9, 2013.

[28] G. E. Torres and T. Mueller, 'Aerodynamic Characteristics of Low Aspect Ratio Wings at Low Reynolds Numbers', Progress in Astronautics and Aeronautics, vol. 195, pp. 115-141, 2001.

[29] V. Modi, 'Moving Surface Boundary-Layer Control: A Review', Journal of Fluids and Structures, vol. 11, no. 6, pp. 627-663, 1997.

[30] H. M. Ali, A. S. M. Rafie and S. A. M. Ali, 'Numerical Analysis of Leading Edge Cylinder Aerofoil on Selig S1223 for Moving Surface Boundary Control'," Journal of Aeronautics, Astronautics and Aviation, vol. 53, no. 2, pp. 143-153, 2021.

[31] A. Mgaidi, A. Rafie, K. Ahmad, R. Zahari, M. A. Hamid and O. Marzuki, 'Numerical and Experimental Analyses of the Flow Around a Rotating Circular Cylinder at Subcritical Regime of Reynolds Number using k-ε and k-ω-sst Turbulent Models', ARPN Journal of Engineering and Applied Sciences, vol. 13, no. 3, pp. 954-960, 2018.

[32] F. R. Menter, 'Two-equation Eddy-viscosity Turbulence Models for Engineering Applications', AIAA Journal, vol. 32, no. 8, pp. 1598-1605, 1994.

[33] D. C. Wilcox, 'Reassessment of the Scale-Determining Equation for Advanced Turbulence Models', AIAA Journal, vol. 26, no. 11, pp. 1299-1310, 1988.

[34] Q. Yao, C. Zhou and C. Wang, 'Numerical Study of the Flow Past a Rotating Cylinder at Supercritical Reynolds Number', Proceedings of 4th International Conference on Mechanical Materials and Manufacturing Engineering, Wuhan, China, October 2016.

[35] J. Anderson, Fundamentals of Aerodynamics. McGraw Hill, 2011.